Atmos. Chem. Phys. Discuss., 15, 22013–22045, 2015
www.atmos-chem-phys-discuss.net/15/22013/2015/
doi:10.5194/acpd-15-22013-2015

Atmospheric Chemistry and Physics Discussions

Variability of water vapour in the Arctic stratosphere

L. Thölix[1], L. Backman[1], R. Kivi[2], and A. Karpechko[3]

[1]Climate Research, Finnish Meteorological Institute, Helsinki, Finland
[2]Arctic Research, Finnish Meteorological Institute, Sodankylä, Finland
[3]Arctic Research, Finnish Meteorological Institute, Helsinki, Finland

Received: 11 June 2015 – Accepted: 23 July 2015 – Published: 17 August 2015

Correspondence to: L. Thölix (laura.tholix@fmi.fi)

Published by Copernicus Publications on behalf of the European Geosciences Union.

Abstract

This study evaluates the stratospheric water vapour distribution and variability in the Arctic. A FinROSE chemistry climate model simulation covering years 1990–2013 is compared to observations (satellite and frostpoint hygrometer soundings) and the sources of stratospheric water vapour are studied. According to observations and the simulations the water vapour concentration in the Arctic stratosphere started to increase after year 2006, but around 2011 the concentration started to decrease. Model calculations suggest that the increase in water vapour during 2006–2011 (at 56 hPa) is mostly explained by transport related processes, while the photochemically produced water vapour plays a relatively smaller role. The water vapour trend in the stratosphere may have contributed to increased ICE PSC occurrence. The increase of water vapour in the precense of the low winter temperatures in the Arctic stratosphere led to more frequent occurrence of ICE PSCs in the Arctic vortex. The polar vortex was unusually cold in early 2010 and allowed large scale formation of the polar stratospheric clouds. The cold pool in the stratosphere over the Northern polar latitudes was large and stable and a large scale persistent dehydration was observed. Polar stratospheric ice clouds and dehydration were observed at Sodankylä with accurate water vapour soundings in January and February 2010 during the LAPBIAT atmospheric sounding campaign. The observed changes in water vapour were reproduced by the model. Both the observed and simulated decrease of the water vapour in the dehydration layer was up to 1.5 ppm.

1 Introduction

Water vapour is the most important natural greenhouse gas in the atmosphere accounting for about half of the current greenhouse effect (Schmidt et al., 2010). Although the majority of water vapour resides in the troposphere, it has been highlighted that stratospheric water vapour variations may play an important role in the decadal scale

ACPD
15, 22013–22045, 2015

variability of the climate (Solomon et al., 2010). Recently the existence of a positive stratospheric water vapour feedback was shown based on observations, i.e. stratospheric water vapour increases with tropospheric temperature, which contributes to the climate sensitivity (e.g., Dessler et al., 2013). Therefore, investigating the changes in stratospheric water vapour abundance is helpful in the detection and attribution of the ongoing climate change.

Water vapour is also an important constituent in the stratospheric chemistry. It intensifies ozone destruction both by producing odd-hydrogen species, which can destroy odd-oxygen, and by formation of polar stratospheric clouds (PSC), which enable efficient conversion of halogen reservoir species to halogen radicals. In the winter polar vortex, water vapour condenses to form type II PSCs (ICE PSCs). ICE PSC formation leads to heterogeneous chlorine activation and ozone depletion (e.g., Solomon et al., 1986). However, Kirner et al. (2015) show that the most efficient ozone destroyer are the heterogeneous reactions on liquid particles. In the high latitudes also the chlorine activation on the ICE particles have a remarcable role. Heterogeneous chemistry on NAT particles causes only a minor part of the ozone depletion. When ice particles sediment to lower altitudes, the reduction of water vapour, i.e. dehydration occurs (Kelly et al., 1989). At the same time the airmasses are effectively denitrified (Hanson and Mauersberger, 1988), which prolong the ozone depletion in the spring.

The Arctic polar vortex is often less stable and maintains higher temperatures than its Antarctic counterpart, and thus ICE PSCs and dehydration are seldom observed. However, increased radiative cooling in the stratosphere, due to the increase of CO_2, as well as an increase in stratospheric water vapour, due to climate change caused warming of the tropical tropopause can enhance the PSC formation. The increased PSCs could lead to more severe ozone depletion (e.g., Kirk-Davidoff et al., 1999) and delay then the ozone recovery (Tian et al., 2009).

The stratospheric water vapour concentration is controlled by atmospheric dynamics and photochemistry. Its main sources are intrusion from the troposphere via the tropical tropopause (Brewer, 1949) and production through methane oxidation

ACPD
15, 22013–22045, 2015

(Bates and Nicolet, 1950; Le Texier et al., 1988). When rising air masses pass through the cold tropical tropopause region, moisture is removed due to freezing and sedimentation (Brewer, 1949). The variability in the entry of water vapour into the stratosphere is therefore controlled by the variability in the tropical cold point temperature. The oxidation of methane leads to formation of water through a series of reactions. The reaction with OH is the dominating methane loss reaction through most of the stratosphere, while the reaction with excited oxygen becomes increasingly important above 30 km, and photolysis is dominant above 65 km (Le Texier et al., 1988). In addition, the reaction with atomic chlorine has some significance as a sink for methane, but also as a termination reaction of ozone depleting cycles especially in the Antarctic vortex where denitrification reduces the importance of the reaction between ClO and NO_2 (Fahey et al., 1990).

Due to the cold tropical tropopause, only a small fraction of tropospheric water vapour propagates to the stratosphere. As a result, the stratosphere is very dry, but it exhibits considerable variability both in space and time. The large gradient especially over the tropopause makes observation of stratospheric water vapour challenging. The observational challenges mean that long-term time series of stratospheric water vapour are rare, which complicates the study of concentration trends. Frostpoint hygrometer soundings have been performed in Boulder, Colorado, since 1980 and for shorter periods of time also in other locations, including Sodankylä, Finland (Oltmans et al., 2000). Additionally, global data is available from satellite instruments, but only for a limited time span. For example, the Microwave Limb Sounder (MLS) on board the Upper Atmosphere Research Satellite (UARS) (1991–1993) and the Earth Observing System on Aura (EOS-Aura) (2004–today) allows a continuous monitoring of the northern hemispheric stratospheric water vapour distribution since 2004 (e.g., Lambert et al., 2007). Also SAGE II, HALOE, SMR, SCIAMACHY, MIPAS, and ACE-FTS have measured stratospheric water vapour in the Northern high latitudes, but the spatial and temporal coverage is limited.

ACPD
15, 22013–22045, 2015

Several studies have used these available measurements to look into water vapour trends, especially in the mid-latitudes. Oltmans et al. (2000) analysed frostpoint hygrometer measurements above Boulder Colorado and reported a trend of about $+0.048 \pm 0.001\,\mathrm{ppm\,yr^{-1}}$ between 1980 and 2000 at level 18–20 km. Randel et al. (2004) compared the Boulder data to the HALOE measurements and reported differences between the Boulder data set and HALOE water vapour data. The seasonal and interannual changes were comparable, but the long term increase observed in soundings were not shown in HALOE data. Later Scherer et al. (2008) did corrections for the instrumental bias of the Boulder frostpoint hygrometer data and updated the Boulder trend and reported a trend of $+0.03$–$0.04\,\mathrm{ppm\,yr^{-1}}$ between 1980 and 2000 at the same altitude, but noted a sudden drop in the stratospheric water vapour beginning in 2001. Hurst et al. (2011) presented a new trend analysis of the 30 year record of Boulder stratospheric water vapour measurements (1980–2010) and found a +1.0 ppm increase over that time period at 16–26 km altitude, with significant shorter term variations. However, Hegglin et al. (2014) suggested, based on merged satellite data set, that the Boulder time series is not globally representative and instead reported negative trends in mid- and high latitudes at 16 km altitude between the end of 1980s and 2010. Negative trends in Boulder and generally in the mid-latitudes at 18 km altitude between 2000 and 2009 have also been reported in previous studies (e.g., Solomon et al., 2010). On the other hand, due to the lack of long term time series, there have been very few studies of stratospheric water vapour trends in the Arctic, where variations in the water content can have large effects on spring-time ozone depletion. Recently Hegglin et al. (2013) have compared water vapour climatologies from 13 satellite products within the SPARC data initiative and analysed also the anomalies in the Northern extratropics water vapour. They found that the uncertainty in water vapour increases toward the polar regions and the mesosphere and the UTLS region.

In this study, we use the FinROSE chemistry transport model (FinROSE-ctm) (Damski et al., 2007; Thölix et al., 2010) to investigate the stratospheric water vapour in the Arctic for the period 1990–2013. In Sect. 3 we describe the water vapour distri-

ACPD
15, 22013–22045, 2015

bution in FinROSE simulations and observations. The modelled water vapour is evaluated against soundings at Sodankylä, Finland (67.4° N, 26.6° E) and MLS satellite observations. The studied period includes the exceptionally cold January 2010 Arctic vortex with large scale ICE PSC formation, which was observed also by the CALIPSO space-borne lidar (Pitts et al., 2011). Section 4 shows the long term variations of water vapour and its sources. Section 5 describes the dehydration frequency in the Arctic stratosphere from 1990 to 2013. Section 6 deals with the Arctic winter 2010, including results from the LAPBIAT atmospheric sounding campaign.

2 Modelling and data

2.1 FinROSE

The FinROSE-ctm (Damski et al., 2007) is a global off-line chemistry-transport model describing the stratosphere and mesosphere. The model produces the distribution of 36 species and the chemistry scheme describes 110 gas phase reactions and 37 photodissociation processes. The PSC scheme includes liquid binary aerosols (LBA), super-cooled ternary solutions (STS, type Ib) and solid nitric acid trihydrate (NAT, type Ia) and ice (ICE, type II) PSCs. The model chemistry includes altogether 30 heterogeneous reactions on/in liquid binary aerosols and type Ia, Ib and II PSCs. Particle sedimentation, leading to dehydration and denitrification of the stratosphere, is also included in the model. The heterogeneous chemistry scheme in FinROSE is based on the calculation of the composition and volume of sulphate aerosols and PSCs and the partitioning of species between gas phase and condensed phase. The number density profile is prescribed for each PSC type (Damski et al., 2007) and the sulphuric acid distribution [$\mu m^2\ cm^{-3}$] is based on 2-D model data (Bekki and Pyle, 1992). The chemical kinetics used in this work follow the recommendations by Sander et al. (2011) and Atkinson et al. (2007). Photodissociation coefficients were calculated using the PHODIS radiative transfer model (Kylling et al., 1997) and were used in the

ACPD
15, 22013–22045, 2015

model through look-up tables. The model transport is calculated using a flux-form semi-lagrangian transport scheme (Lin and Rood, 1996).

The tropospheric concentrations of the chemical species is prescribed via model boundary conditions. Tropospheric water vapour and ozone were obtained from the ECMWF ERA-Interim reanalysis (Simmons et al., 2007; Dee et al., 2011). Tropospheric methane (CH_4) is from Global view-data (ftp://aftp.cmdl.noaa.gov/products/globalview/ch4/), nitrous oxide (N_2O) from Agage data (Prinn et al., 2000), and halogens (Cly and Bry) are from Montzka et al. (2009) updated data. Carbon dioxide CO_2 is based on global annual mean trend data (ftp://aftp.cmdl.noaa.gov/products/trends/co2). At the upper model boundary (0.1 hPa), climatological values averaged over 2005–2013 from MLS data were used for water vapour and ozone. The model has also a tracer aimed for water vapour studies; a chemically passive tracer for describing the amount of water vapour entering through the tropopause.

In this study, the model was run with a horizontal resolution of $6^\circ \times 3^\circ$ (longitude × latitude) at 35 hybrid-sigma levels, from the surface up to 0.1 hPa (about 65 km). The wind, temperature and surface pressure fields were obtained from the European Centre for Medium-range Weather Forecasts (ECMWF) ERA-Interim reanalyses (Dee et al., 2011).

2.1.1 Water vapour and PSC measurements

Accurate measurements of stratospheric water vapour from the northern high latitudes are rare; however, such soundings are available at Sodankylä (67.4° N, 26.6° E), northern Finland since early 2000 (Vömel et al., 2007a, c). Sodankylä site is representative of high latitude conditions in the northern Europe, and the upper air soundings in winter and spring sample air both inside and outside the polar stratospheric vortex. Here we have used stratospheric water vapour measurements from two atmospheric sounding campaigns. First set of observations was obtained during the Lapland Atmosphere–Biosphere Facility (LAPBIAT) Upper Tropospheric Lower Stratospheric Water Vapour Validation Project (LAUTLOS-WAVVAP) campaign in early 2004 (e.g.,

ACPD
15, 22013–22045, 2015

Deuber et al., 2005; Vömel et al., 2007a, b; Karpechko et al., 2007; Suortti et al., 2008). The second campaign (the LAPBIAT–2 (Lapland Atmosphere–Biosphere Facility) Atmospheric Sounding Campaign) took place in January–March 2010 (Kivi et al., 2010; Khaykin et al., 2013; Engel et al., 2014; Grooß et al., 2014). During these campaigns three types of water vapour instruments were flown. The NOAA frostpoint instrument (Oltmans, 1985; Vömel et al., 1995) was flown during the first campaign. First flights of the Cryogenic Frostpoint Hygrometer (CFH) were also performed during the LAUTLOS campaign. The CFH flights were continued during the LAPBIAT-2 campaign in 2010. CFH is a well characterised instrument capable of accurate water vapour measurements in the lower stratosphere typically up to the altitude of 25–28 km (Vömel et al., 2007a). Lyman-alpha fluorescence hygrometers (FLASH-B) were also flown during both campaigns (Vömel et al., 2007b; Khaykin et al., 2013). In this study we have used 13 NOAA frostpoint hygrometer profiles obtained during the first campaign and 13 CFH soundings obtained during the second atmospheric sounding campaign. In addition, one NOAA profile from 2003, two NOAA profiles from 2006, as well as two CFH profiles from 2008 and one CFH profile from 2012 were used.

In addition to the balloon soundings, observations from the Microwave Limb Sounder (MLS) on board the Aura satellite provide global profile measurements of H_2O, temperature and several trace gases (Lambert et al., 2007). In this study, we use the MLS version 3.3 Level 2 data, which are available from August 2004 to present. The Level 2 data are produced on pressure surfaces from 316 to 0.1 hPa with a vertical resolution of about 3 km. Each day about 3500 vertical profiles are measured along a sun-synchronous suborbital track. We also used polar stratospheric cloud observations provided by the Cloud-Aerosol Lidar and Infrared Pathfinder Satellite Observation (CALIPSO) space-borne lidar (Pitts et al., 2007). The CALIPSO PSC algorithm classifies PSCs by composition. Six different classes are defined: supercooled ternary solution (STS), two classes of liquid/NAT mixtures and mix 2 enhanced, water ice and wave ice (Pitts et al., 2011). We used these CALIPSO PSC composition classes for calculating the areas where PSCs were observed. The area is calculated separately

ACPD
15, 22013–22045, 2015

for ICE and NAT. Both water ice and wave ice are included in the ICE area and all the NAT mix classes to the NAT area. CALIPSO data is available from June 2006 to present.

3 Water vapour distribution

The FinROSE-ctm has been run using ERA-Interim meteorology and ERA-Interim water vapour data as tropospheric boundary condition. Thus, the evolution of water vapour in the FinROSE model is strongly constrained by the water vapour at the ERA-Interim tropopause. The description of stratospheric H_2O in the ECMWF model is however simplified (Monge-Sanz et al., 2013) and the chemistry scheme in FinROSE can therefore be expected to produce a more realistic water vapour distribution.

First, we evaluated the simulated stratospheric water vapour distribution from FinROSE against measurements above Sodankylä. Figure 1 shows simulated and measured climatologies of water vapour distribution over Sodankylä between 2004 and 2013. Overall, the FinROSE-ctm (top panel) is capable of reproducing the MLS observations (middle panel) of water vapour concentration and its vertical and temporal distributions. The maximum values of water vapour are located at the same altitude in both data sets. The largest differences are in summer, between 10 and 1 hPa, the concentration in FinROSE is about 1 ppm higher compared to MLS. In comparison, the ECMWF ERA-Interim reanalysis (bottom panel) clearly underestimates the observed water vapour concentrations in the upper stratosphere, while the lower stratosphere compares well with MLS. The largest discrepancies are seen in the upper stratosphere where the water vapour is underestimated by 1 ppm. The dryness in the reanalysis data is likely a consequence of cold bias in the tropics in the ERA-Interim data (Schoeberl et al., 2012). Also the methane parameterisation in the ECMWF model lead to too dry air (Dethof, 2003). It is also possible that too fast general circulation previously identified in the ECMWF model causes reduced moisture in the polar regions (Simmons et al., 1999; Schoeberl et al., 2012; Monge-Sanz et al., 2013). The same general

ACPD
15, 22013–22045, 2015

circulation is also in the FinROSE model because ERA-Interim meteorology is used. However, the full chemistry of the FinROSE-ctm improves the water vapour distribution of the model. During winter and spring the very top levels of ERA-Interim are too moist compared to observations. This is probably due to a too low model upper boundary; the ECMWF model does not extend to the upper mesospheric altitudes where photochemical processes destroy water vapour causing the observed dry upper stratosphere. This process is also missing from the FinROSE-ctm; however, it has been indirectly included by using a water vapour climatology calculated from MLS data as an upper boundary condition. Overall, Fig. 1 shows that FinROSE is capable of simulating the distribution and magnitude of stratospheric water vapour in the high northern latitudes, which gives us confidence in its applicability for a more detailed study of water vapour distribution, sources, and long-term variability.

For a more detailed comparison of model results with observations at northern high latitudes, we calculated the average mixing ratios and standard deviations of water vapour profiles above Sodankylä from the FinROSE model, ERA-Interim and observations. We chose January–February, because of the availability of balloon soundings during this time. In this comparison ERA-Interim and FinROSE data are available daily from all the January–February months between 2004 and 2013, MLS almost daily, but soundings are available less frequently (altogether 32 profiles). From FinROSE and ERA-Interim the gridpoint nearest Sodankylä have been chosen. From MLS all the profiles measured in the Sodankylä gridpoint and flagged as good quality are used. Figure 2 compares January–February-mean water vapour mixing ratios above Sodankylä from the FinROSE simulation (black), ECMWF ERA-Interim reanalysis (green), MLS satellite measurements (blue), and frostpoint hygrometer soundings (red). The data are shown for seven different pressure levels; 100, 56, 30, 21, 10, 3 and 1 hPa. Left panel shows the mixing ratios in winter 2010 and right panel shows the relative differences compared to MLS observations calculated over winters 2004–2013. The winter 2010 was chosen for left panel because of the largest amount of soundings.

ACPD
15, 22013–22045, 2015

The modelled water vapour concentration profile agrees well with MLS measurements in winter 2010 (shown in Fig. 2 left panel). The model data is within 0–0.5 ppm of the MLS data, except at 3 hPa where the model gives 0.7 ppm more water vapour. Compared to the Sodankylä soundings, FinROSE has about 0.7 ppm more water vapour at 100 hPa, but the difference decreases with altitude, except at 30 hPa altitude where the model is about 0.7 ppm drier. At the levels between 100 and 21 hPa the soundings fit to the range of variation of MLS. The difference is less than 0.5 ppm. Balloon sounding data are not available above 20 hPa. ERA-Interim is generally drier compared to MLS and soundings throughout the studied altitude range except at level 30 hPa. ERA-Interim water vapour concentration is also always more than 0.7 ppm lower than the FinROSE's as can be expected based on Fig. 1.

The right panel shows the differences between models and observations averaged over several winters. The differences have been calculated using all the available data during Januarys and Februarys between 2004 and 2013. The differences between FinROSE and MLS, ERA-Interim and MLS and soundings and MLS remain smaller than 10 % at all altitudes. ERA-Interim is drier than MLS also in this climatology but FinROSE is moister than MLS. Soundings are also drier compared to MLS, but the difference is smaller than the difference between ERA-Interim and MLS. Sounding vs. model comparisons are complicated, because firstly the number of soundings is limited and secondly, some of the soundings are obtained in the vicinity of the stratospheric vortex. Model to satellite differences have been calculated using all available data, both vortex conditions and non-vortex conditions included.

4 The origin and long term variability of water vapour

The sources of stratospheric water vapour are transport from the tropical troposphere and chemical production mainly from methane oxidation. Water vapour enters the stratosphere through the tropical tropopause and propagates then to the upper altitudes and higher latitudes. The FinROSE model has a tracer for studying these two

ACPD
15, 22013–22045, 2015

water vapour sources. A passive H_2O-tracer, that is not affected by chemistry, represents the transported water vapour. The difference between H_2O-tracer and H_2O represents the amount of water vapour produced by chemistry, i.e. mainly through oxidation of methane, but also hydrogen. Figure 3 shows the fractions of water vapour due to transport (upper panel) and chemistry (lower panel) according to simulations. Transport from the troposphere covers more than a half of the water vapour. At lower altitudes the transported part is clearly the most important. The chemically produced water vapour becomes more important at higher altitudes with a maximum around 1 hPa in the summer and autumn, where the fraction reaches almost 50 %.

The water vapour trend above Sodankylä, was investigated from a FinROSE model simulation covering the years 1986–2013. The first four years were discarded as spin-up and the period 1990–2013 is analysed below. Figure 4 compares monthly-mean water vapour mixing ratios in the Arctic area, 70–90° N from the FinROSE simulation (black line), ECMWF ERA-Interim reanalysis (green line) and MLS satellite measurements (orange line). The data is from 56 hPa level. Throughout the investigated period, the water vapour amount in FinROSE and the observations varies within about 4–5.5 ppm. The modelled water vapour concentration agrees well with MLS measurements from 2005–2008; however, after that FinROSE shows higher concentrations than observed by MLS and thus reveals a stronger increasing trend in these last five years. The growth rate is about 1 ppm decade^{-1} in FinROSE and 0.6 ppm decade^{-1} in MLS. As can be expected based on Fig. 1, the ERA-Interim water vapour concentration is about 0.5 ppm lower than in FinROSE. It is, however, noteworthy that the difference remains approximately the same throughout the study period. The increasing trend from 2007 to 2012 is very similar in FinROSE and ERA-Interim data, resulting from the use of ERA-Interim meteorology as driver data in the FinROSE simulation.

Panels b–e in Fig. 4 show the anomaly of FinROSE water vapour and the sources of it between latitudes 70–90° N. The anomaly of water vapour concentration is shown with a black line. The red line is the anomaly of the passive water vapour tracer and the blue line is the anomaly of the chemically produced part of water. The green line shows

ACPD
15, 22013–22045, 2015

the anomaly of ECMWF ERA-Interim water vapour for comparison. All the anomalies are calculated from monthly mean data and the climatology for anomaly calculations has been calculated over the years 1994–2013. The altitudes of the panels are 1, 10, 56 and 100 hPa. At the 1 and 10 hPa pressure levels there is no clear trend in the water vapour before 2008. After that the anomaly of water vapour is positive and stays positive until the end of the timeseries. At the lower altitudes, levels 56 and 100 hPa, there is decrease in the water vapour in the beginning of the time series, until year 1998. After that the water vapour anomaly does not show any trend until the mid 2000's. In the latter part of the decade the water vapour values starts to increase, however the most recent years again show a decrease in water vapour.

Solomon et al. (2010) found a positive trend in the water vapour data until about year 2000 and negative after that over Boulder at the mid-latitudes around 80 hPa. Hegglin et al. (2014) showed that the water vapour trends over Boulder should not be considered representative of the global stratosphere. In the FinROSE model results for the high northern latitudes the long term change of water vapour is positive. The water vapour trends for mid-latitudes and tropics in FinROSE develop similarly as in higher latitudes (not shown). The anomalies seen in FinROSE also agree with the results by Dessler et al. (2013) for tropical water vapour between 2005 and 2013. Also the approximately two year periodicity seen before year 2008 is similar as in the Dessler et al. (2013); Hegglin et al. (2013) and Randel et al. (2004) studies and is related to the tropopause temperature changes associated with the quasi-biennal oscillation (QBO). The QBO-signal has an influence on high latitude water vapour due to mixing processes. After 2008 the signal weakens at the high latitudes.

The Sodankylä water vapour concentration in FinROSE-ctm increases by about 0.8 ppm at altitude 56 hPa from year 2004 until year 2012. This increase corresponds to ca 1 K increase in the frostpoint temperature (Marti and Mauersberger, 1993). However, the concentration during recent years (2012 to 2014) has decreased more than 0.5 ppm. The FinROSE water vapour anomaly (black line in the Fig. 4) and the passive tracer anomaly (red line) have nearly the same changes as the water vapour, in

ACPD
15, 22013–22045, 2015

line with the results presented in Fig. 1. The evolution of the FinROSE water vapour anomaly is similar to the ERA-Interim anomaly (green line), which is expected as the FinROSE-ctm is driven by the ERA-Interim data. The chemical part (blue line) has only a small positive trend consistent with previous studies, because the tropospheric methane concentration was nearly stable in the analysed time period. The increase in the tropospheric methane concentration since 2007 is only about 0.05 ppm. Furthermore, the effect of tropospheric methane concentrations on statospheric water vapour is seen with a delay.

5 Arctic dehydration frequency

In the polar vortex areas the concentration of water vapour can be changed also by dehydration. Water freezes into ice particles, sediments to lower altitudes and sublimates. Dehydration is frequently observed in the Antarctic polar vortex and there the magnitude of decrease of the water vapour by dehydration is several ppms. The water vapour mixing ration can be reduced to 1.5 ppm in the cold stable Antarctic vortex (Vömel et al., 1995). In the Arctic vortex the dehydration is rare, because the temperatures are higher. However, ICE PSCs are formed also in the Arctic vortex and it is possible for dehydration to occur.

ICE PSC formation is controlled by temperature and water vapour concentration, which both exhibit considerable variability. FinROSE simulates significant ICE PSC conditions in the Arctic in 10 out of 24 winters (1990, 1993, 1995, 1996, 2000, 2005, 2008, 2010, 2011 and 2012), which gives an average frequency of 0.4 per winter. However, they cover only a small fraction of the vortex. The largest extent of simulated ICE PSCs was seen in 1990, with an area of 3×10^6 km^2 at 56 hPa. In 1993, 2005, 2011 and 2012 an area of around 2.5×10^6 km^2 were reached. Figure 5 shows the area of the gridpoints where ICE PSC (black) and NAT (green) form in the FinROSE model at 56 hPa. From 2007 onwards the PSC areas from CALIPSO lidar observations are shown as comparison, ICE in red and NAT in blue. Based on the timeseries in Fig. 5

ACPD
15, 22013–22045, 2015

it seems that there is an increase in ICE PSCs in the recent winters. Between 2008 and 2013 there are 4 ICE PSC winters in 6 years, which leads to frequency 0.67. This is likely a result of cold conditions and the increase in the water vapour concentration. Both the temperature and water vapour have varied, and especially the variability in the temperature has been large. The PSC areas in FinROSE agrees well with the ones calculated from CALIPSO data. However in some cases, e.g. beginning of winters, CALIPSO detects PSCs that are not simulated by FinROSE. This may indicate a warm bias in ERA-Interim in that period. Also in 2007 CALIPSO detects ICE PSCs, which are not seen in the model. This might be due to the resolution of the model (3×6), as the areas are quite small. NATs are more common than ICE PSCs in the Northern high latitudes and they are simulated yearly. CALIPSO detects NATs at the same times as in the FinROSE simulations, but the areas are larger in the simulations.

Figure 6 shows the relation of the area of simulated (and observed) ICE PSCs and the area of colder than 190 K temperatures in January at level 56 hPa. One point (or cross) denotes one January day between 2007 and 2013 in FinROSE simulation (CALIPSO observation). The colour of the marks show the water vapour concentration averaged in the vortex. It can be seen that the cold temperatures are not enough for the ICE PSC formation. Higher water vapour concentrations produce larger areas of ICE PSC and in dry vortex no ICE PSCs form although the temperature is low enough. The cold temperature areas as well as the ICE PSC areas are larger in FinROSE than in CALIPSO. The difference is not so remarkable in case of ICE PSCs. CALIPSO detects small ICE PSC areas with small cold temperature areas, but in case of FinROSE the ICE PSCs are not allways created although the cold temperature area is large. The increase of water vapour in the vortex area have been more than 0.5 ppm after 2007. That would have increased the size of ICE PSC areas even if the temperatures have been the same.

ACPD
15, 22013–22045, 2015

6 Case study: winter 2009/2010

The winter 2009/2010 was unusually cold in the Arctic polar region. The temperature were below 190 K in a large area of the polar vortex. Temperatures below 195 K were simulated even south of 60° N. PSCs were formed and even persistent dehydration was observed over Northern polar latitudes for the first time (Khaykin et al., 2013). The vortex lasted until the beginning of April, and near Sodankylä until 11 February. Colder than 195 K air occurred until the end of January 2010. After 11 February 2010 the vortex moved towards the south and and a mixing with moister mid-latitude air has occurred.

The FinROSE-ctm simulation was studied more thoroughly for the winter 2009/2010. The results were also compared to observations. Cold temperatures occurred between 20 and 28 km in the ERA-Interim data and cold temperatures can be seen also in measured temperatures. Also a reduction of water vapour at around 56 hPa, seen both in the simulations and in observations, can be attributed to the formation of ICE PSCs. Indeed, also ICE PSC particles were simulated at 22–24 km by the model and also seen in the balloon sounding data from the LAPBIAT campaign (Khaykin et al., 2013).

Figure 7 shows the area of ICE and NAT PSCs and the evolution of temperature above Sodankylä in the 2009/2010 winter. ICE PSCs occur same time, at the coldest dates both in FinROSE simulations and CALIPSO observations. ICE PSC areas in CALIPSO are larger than in FinROSE, but the clouds are seen at the same altitudes. Especially the ICE PSC episodes in beginning of January 2010 are clearly weaker in FinROSE than in CALIPSO. The second row shows the area of NAT PSCs. FinROSE simulates larger areas than CALIPSO detects. Also the altitude differs; the maximum area of NAT PSCs in FinROSE is at 20 km altitude but at 22 km in the CALIPSO data. The timing is comparable. The Sodankylä temperatures in ERA-Interim and CALIPSO are nearly the same, but can still cause some differences to the PSCs. The differences might be explained also by the model resolution and the simplicity of the PSC parameterization and the gridding of CALIPSO data.

ACPD
15, 22013–22045, 2015

Figure 8 shows maps of temperature from ERA-Interim, frostpoint temperature from FinROSE and MLS and ICE PSC from FinROSE and CALIPSO from Northern Hemisphere vortex area between 17 and 23 January 2010 at level 56 hPa. The minimum temperatures in the vortex (first row) are very low in this time period, even below 188 K. In this figure the water vapour mixing ratios from FinROSE and MLS are shown as frostpoint temperatures. The frostpoint temperature from FinROSE-ctm (second row) is the highest at the vortex boundary and the lowest in the middle of the vortex. The driest areas coincide both in space and time with the coldest temperatures. The MLS frostpoint temperature (third row, 3 day average) also show the same dry areas as FinROSE. Areas with very cold temperatures correlates with very low water vapour content areas because of ICE PSC formation. The water vapour is condensed into ice particles, which are sedimented downwards resulting in dehydrated air masses. The next two rows in Fig. 8 show the area where ICE PSCs are simulated in FinROSE at 56 hPa altitude and observed by CALIPSO also around 56 hPa. ICE PSCs can be seen in large areas in the vortex in the FinROSE simulation. ICE PSCs are seen in the areas in the CALIPSO observations, but the data coverage of the observations makes the shape less uniform.

The bottom row in Fig. 8 shows modelled frostpoint temperature profiles above Sodankylä from FinROSE-ctm and temperature profiles from ECMWF ERA-Interim analysis, frostpoint temperature calculated from MLS satellite water vapour and frostpoint temperature from Sodankylä water vapour soundings. The resolution of the FinROSE simulation used in this study is $6^\circ \times 3^\circ$ and Sodankylä (lon 26.6° E, lat 67.4° N) is located between four grid points. The panels in Fig. 8 represents averaged data from the four nearest grid points from Sodankylä. Overall FinROSE can simulate the frostpoint temperature quite well. The ECMWF ERA-Interim temperature reaches or almost reaches the frostpoint temperature during the analysed time period. Then the formation of ICE PSC is possible also in the FinROSE-ctm. The cold time period lasts until 26 January. The polar vortex is split after the considered time period. The coldest dates in Sodankylä are 17 and 23 January, and very low frostpoint values can be seen above

ACPD
15, 22013–22045, 2015

40 hPa altitudes. The decrease of water vapour is likely a result of dehydration. The water vapour concentration decreases about 1 to 1.5 ppm from the median values. A small increase of water vapour below 40 hPa on 23 January can be a sign of re-hydration. However, it is not visible in the FinROSE results in the gridpoint closest to Sodankylä, but in some colder gridpoints it can be seen.

Winter 2010 was extremely cold and the temperature dropped below the frostpoint temperature. ICE PSCs was formed and observed on several days during the LAPBIAT campaign. The occurence of ICE PSCs were also succesfully simulated.

7 Conclusions

FinROSE has been shown to be capable of simulating the water vapour distribution and evolution in the Northern high latitude stratosphere. The representation of water vapour in FinROSE is improved compared to the ERA-Interim data, even though the ERA-Interim data is used as tropospheric boundary condition. The full chemistry in FinROSE can add the water vapour to the ECMWF ERA-Interim water vapour. The model gives results comparable to the MLS satellite measurements. However, some discrepancies compared to MLS remain.

The concentration of stratospheric water vapour in FinROSE is too high, especially in the summer time. Compared to the Sodankylä frost point hygrometer the model is too moist. However, the number of the comparisons is limited. In addition, some of the soundings have been made in the vicinity of the polar vortex, which further complicates comparison with the model data.

The main sources of the stratospheric water vapour are transport from the tropical troposphere and methane oxidation. A passive tracer was used in the FinROSE model for investigating the relative importance of the different sources of water vapour. The chemically produced fraction shows a maximum at altitudes between 6 and 0.3 hPa. At these altitudes in the summertime the photochemical part is nearly as big as the transported part.

ACPD
15, 22013–22045, 2015

Long term changes can be seen in water vapour below 10 hPa; water vapour increases between 2006 and 2011, which has been followed by a decreasing trend. The increasing trend is about 1 ppm in 5 years. In the upper stratosphere the trend is less clear. In the MLS data the trend is smaller than seen in FinROSE. The trends can be attributed to water vapour transported trough the tropical tropopause. The photochemically produced part of water vapour shows less significant trends, due to comparably smaller changes in the tropospheric methane concentration.

In the FinROSE simulation ICE PSCs occurred in Northern high latitudes at 10 winter of 24 simulated. NAT PSCs were simulated more often, at least a small area every year. CALIPSO instrument has measured PSCs since 2006. FinROSE simulates PSCs generally at the same time as observed by CALIPSO. Also the area of ICE PSCs occurrence comparable to the CALIPSO observations. The NAT PSC area is larger in FinROSE than in CALIPSO. Both PSC types have become more frequent in recent years of the simulation. ICE PSC occurrence depends on the temperature and the amount of water in the stratosphere. The area of colder than 190 K is much larger than the area of simulated ICE PSCs in FinROSE or the area of detected ICE with CALIPSO. Increased stratospheric water vapour concentration in high latitudes may have increased the ICE PSC occurrence after year 2006.

The winter 2009/2010 was extremely cold in the Arctic stratosphere. At Sodankylä ICE PSCs were observed. The ICE PSCs caused dehydration and rehydration at lower altitudes. Balloon borne water vapour measurements were done at Sodankylä in winter–spring 2010. ICE PSCs were observed together with significant H_2O-reduction during the coldest period of January 2010. More than 1 ppm reduction of water vapour was seen in the balloon borne sonde profiles as well as in the model simulations.

Acknowledgements. We want to thank the UARS reference atmosphere project and MLS/AURA teams for water vapour data and the Atmospheric Science Data Center for the CALIPSO data. The MLS data were obtained through the Aura MLS website (http://mirador.gsfc.nasa.gov/). CALIPSO data were obtained from the NASA Langley Research Center At-

ACPD
15, 22013–22045, 2015

mospheric Science Data Center. The Sodankylä water vapour sounding providers are also thanked. The funding from the Academy of Finland through the UTLS project (140408) is gratefully acknowledged.

References

Atkinson, R., Baulch, D. L., Cox, R. A., Crowley, J. N., Hampson, R. F., Hynes, R. G., Jenkin, M. E., Rossi, M. J., and Troe, J.: Evaluated kinetic and photochemical data for atmospheric chemistry: Volume III – gas phase reactions of inorganic halogens, Atmos. Chem. Phys., 7, 981–1191, doi:10.5194/acp-7-981-2007, 2007. 22018

Bates, D. R. and Nicolet, M.: The photochemistry of water vapor, J. Geophys. Res., 55, 301–327, 1950. 22016

Bekki, S. and Pyle, J.: Two-dimensional assessment of the impact of aircraft sulphur emissions on the stratospheric sulphate aerosol layer, J. Geophys. Res., 9, 15839–15847, 1992. 22018

Brewer, A. W.: Evidence for a world circulation provided by the measurements of helium and water vapor distribution in the stratosphere, Q. J. Roy. Meteor. Soc., 75, 351–363, 1949. 22015, 22016

Damski, J., Thölix, L., Backman, L., Taalas, P., and Kulmala, M.: FinROSE – middle atmospheric chemistry and transport model, Boreal Environ. Res., 12, 535–550, 2007. 22017, 22018

Dee, D. P., Uppala, S. M., Simmons, A. J., Berrisford, P., Poli, P., Kobayashi, S., Andrae, U., Balmaseda, M. A., Balsamo, G., Bauer, P., Bechtold, P., Beljaars, A. C. M., van de Berg, L., Bidlot, J., Bormann, N., Delsol, C., Dragani, R., Fuentes, M., Geer, A. J., Haimberger, L., Healy, S. B., Hersbach, H., Holm, E. V., Isaksen, L., Kallberg, P., Kohler, M., Matricardi, M., McNally, A. P., Monge-Sanz, B. M., Morcrette, J.-J., Park, B.-K., Peubey, C., de Rosnay, P., Tavolato, C., Thepaut, J.-N., and Vitart, F.: The ERA-Interim reanalysis: configuration and performance of the data assimilation system, Q. J. Roy. Meteorol. Soc., 137, 553–597, 2011. 22019

Dethof, A.: Aspects of modelling and assimilation for the stratosphere at ECMWF, SPARC Newslett., 2, 11–14, 2003. 22021

Deuber, B., Haefele, A., Feist, D. G., Martin, L., Kampfer, N., Nedoluha, G. E., Yushkov, V., Khaykin, S., Kivi, R., and Vömel, H.: Middle Atmospheric Watre Vapor Radiometer (MIAWARA): validation and first results of the LAPBIAT Upper Tropospheric Lower Stratospheric

ACPD
15, 22013–22045, 2015

Water Vapor Validation Project (LAUTLOS-WAVVAP) campaign, J. Geophys. Res., 110, D13306, doi:10.1029/2004JD005543, 2005. 22020
Dessler, A. E., Schoeberl, M. R., Wang, T., Davis, S. M., and Rosenlof, K. H.: Stratospheric water vapor feedback, P. Natl. Acad. Sci. USA, 45, 18087–18091, doi:10.1073/pnas.1310344110, 2013. 22015, 22025
Engel, I., Luo, B. P., Khaykin, S. M., Wienhold, F. G., Vömel, H., Kivi, R., Hoyle, C. R., Grooß, J.-U., Pitts, M. C., and Peter, T.: Arctic stratospheric dehydration – Part 2: Microphysical modeling, Atmos. Chem. Phys., 14, 3231–3246, doi:10.5194/acp-14-3231-2014, 2014. 22020
Fahey, D. W., Kelly, K. K., Kawa, S. R., Tuck, A. F., Loewenstein, M., Chan, K. R., and Heidt, L. E.: Observations of denitrification and dehydration in the winter polar stratospheres, Nature, 344, 321–324, doi:10.1038/344321a0, 1990. 22016
Grooß, J.-U., Engel, I., Borrmann, S., Frey, W., Günther, G., Hoyle, C. R., Kivi, R., Luo, B. P., Molleker, S., Peter, T., Pitts, M. C., Schlager, H., Stiller, G., Vömel, H., Walker, K. A., and Müller, R.: Nitric acid trihydrate nucleation and denitrification in the Arctic stratosphere, Atmos. Chem. Phys., 14, 1055–1073, doi:10.5194/acp-14-1055-2014, 2014. 22020
Hanson, D. and Mauersberger, K.: Vapor pressures of HNO_3/H_2O solutions at low temperatures, J. Phys. Chem., 92, 6167–6170, 1988. 22015
Hegglin, M., Tegtmeier, S., Anderson, J., Froidevaux, L., Fuller, R., Funke, B., Jones, A., Lingenfelser, G., Lumpe, J., Pendlebury, D., Remsberg, E., Rozanov, A., Toohey, M., Urban, J., von Clarmann, T., Walker, K. A., Wang, R., and Weigel, K.: SPARC Data Initiative: comparison of water vapor climatologies from international satellite limb sounders, J. Geophys. Res., 118, 11824–11846, doi:10.1002/jgrd.50752, 2013. 22017, 22025
Hegglin, M. I., Plummer, D. A., Shepherd, T. G., Scinocca, J. F., Anderson, J., Froidevaux, L., Funke, B., Hurst, D., Rozanov, A., Urban, J., von Clarmann, T., Walker, K. A., Wang, H. J., Tegtmeier, S., and Weigel, K.: Vertical structure of stratospheric water vapour trends derived from merged satellite data, Nat. Geosci., 7, 768–776, doi:10.1038/ngeo2236, 2014. 22017, 22025
Hurst, D. F., Oltmans, S. J., Vömel, H., Rosenlof, K. H., Davis, S. M., Ray, E. A., Hall, E. G., and Jordan, A. F.: Stratospheric water vapor trends over Boulder, Colorado: analysis of the 30 year Boulder record, J. Geophys. Res., 116, D02306, doi:10.1029/2010JD015065, 2011. 22017
Karpechko, A., Lukyanov, A., Kyrö, E., Khaikin, S., Korshunov, L., Kivi, R., and Vömel, H.: The water vapour distribution in the Arctic lowermost stratosphere during the LAUTLOS cam-

ACPD
15, 22013–22045, 2015

paign and related transport processes including stratosphere-troposphere exchange, Atmos. Chem. Phys., 7, 107–119, doi:10.5194/acp-7-107-2007, 2007. 22020

Kelly, K. K., Tuck, A. F., Murphy, D. M., Proffitt, M. H., Fahey, D. W., Jones, R. L., Mckenna, D. S., Loewenstein, M., Podolske, J. R., Strahan, S. E., Ferry, G. V., Chan, K. R., Vedder, J. F., Gregory, G. L., Hypes, W. D., Mccormick, M. P., Browell, E. V., and Heidt, L. E.: Dehydration in the lower Antarctic stratosphere during late winter and early spring, 1987, J. Geophys. Res, 94, 11317–11357, doi:10.1029/JD094iD09p11317, 1989. 22015

Khaykin, S. M., Engel, I., Vömel, H., Formanyuk, I. M., Kivi, R., Korshunov, L. I., Krämer, M., Lykov, A. D., Meier, S., Naebert, T., Pitts, M. C., Santee, M. L., Spelten, N., Wienhold, F. G., Yushkov, V. A., and Peter, T.: Arctic stratospheric dehydration – Part 1: Unprecedented observation of vertical redistribution of water, Atmos. Chem. Phys., 13, 11503–11517, doi:10.5194/acp-13-11503-2013, 2013. 22020, 22028

Kirk-Davidoff, D. B., Anderson, J. G., Hintsa, E. J., and Keith, D. W.: The effect of climate change on ozone depletion through changes in stratospheric water vapour, Nature, 402, 399–401, 1999. 22015

Kirner, O., Müller, R., Ruhnke, R., and Fischer, H.: Contribution of liquid, NAT and ice particles to chlorine activation and ozone depletion in Antarctic winter and spring, Atmos. Chem. Phys., 15, 2019–2030, doi:10.5194/acp-15-2019-2015, 2015. 22015

Kivi, R., Vömel, H., Immler, F., Lehtola, T., Kämpfer, N., Straub, C., Yushkov, V., Khaykin, S., Christensen, T., and Wienhold, F. G.: LAPBIAT atmospheric sounding campaign in 2010, upper-air and remote sensing observations of water vapour, in: WMO Technical Conference on Meteorological and Environmental Instruments and Methods of Observation (TECO-2010), Helsinki, Finland, 30 August–1 September 2010, Instruments and Observing System Methods Report No. 104, WMO/TD-No. 1546, 2010. 22020

Kylling, A., Albold, A., and Seckmeyer, G.: Transmittance of a cloud is wavelength – dependent in the UV-range: physical interpretation, Geophys. Res. Lett., 24, 397–400, doi:10.1029/97GL00111, 1997. 22018

Lambert, A., Read, W. G., Livesey, N. J., Santee, M. L., Manney, G. L., Froidevaux, L., Wu, D. L., Schwartz, M. J., Pumphrey, H. C., Jimenez, C., Nedoluha, G. E., Cofield, R. E., Cuddy, D. T., Daffer, W. H., Drouin, B. J., Fuller, R. A., Jarnot, R. F., Knosp, B. W., Pickett, H. M., Perun, V. S., Snyder, W. V., Stek, P. C., Thurstans, R. P., Wagner, P. A., Waters, J. W., Jucks, K. W., Toon, G. C., Stachnik, R. A., Bernath, P. F., Boone, C. D., Walker, K. A., Urban, J., Murtagh, D., Elkins, J. W., and Atlas, E.: Validation of the Aura Microwave Limb

ACPD
15, 22013–22045, 2015

Sounder middle atmosphere water vapor and nitrous oxide measurements, J. Geophys. Res., 112, D24S36, doi:10.1029/2007JD008724, 2007. 22016, 22020
Le Texier, H., Solomon, S., and Garcia, R. R.: The role of molecular hydrogen and methane oxidation in the water vapour budget of the stratosphere, Q. J. Roy. Meteorol. Soc., 114, 281–295, 1988. 22016
Lin, S.-J. and Rood, R. B.: Multidimensional flux-form semi-lagrangian transport schemes, Mon. Weather Rev., 124, 2046–2070, 1996. 22019
Marti, J. and Mauersberger, K.: A survey and new measurements of ice vapor pressure at temperatures between 170 and 250 K, Geophys. Res. Lett., 20, 363–366, doi:10.1029/93GL00105, 1993. 22025
Monge-Sanz, B. M., Chipperfield, M. P., Untch, A., Morcrette, J.-J., Rap, A., and Simmons, A. J.: On the uses of a new linear scheme for stratospheric methane in global models: water source, transport tracer and radiative forcing, Atmos. Chem. Phys., 13, 9641–9660, doi:10.5194/acp-13-9641-2013, 2013. 22021
Montzka, S. A., Butler, J. H., Elkins, J. W., Thompson, T. M., Clarke, A. D., and Lock, L. T.: Present and future trends in the atmospheric burden of ozone-depleting halogens Nature, 398, 690–694, 1999. 22019
Oltmans, S. J.: Measurements of water vapor in the stratosphere with a frost point hygrometer, measurement and control in science and industry, in: Proceedings of the 1985 International Symposium on Moisture and Humidity, Instrument Society of America, Washington, DC, 251–258, 1985. 22020
Oltmans, S. J., Vömel, H., Hofmann, D. J., Rosenlof, K. H., and Kley, D.: The increase in stratospheric water vapor from balloonborne, frostpoint hygrometer measurements at Washington, D. C., and Boulder, Colorado, Geophys. Res. Lett., 27, 3453–3456, doi:10.1029/2000GL012133, 2000. 22016, 22017
Pitts, M. C., Thomason, L. W., Poole, L. R., and Winker, D. M.: Characterization of Polar Stratospheric Clouds with spaceborne lidar: CALIPSO and the 2006 Antarctic season, Atmos. Chem. Phys., 7, 5207–5228, doi:10.5194/acp-7-5207-2007, 2007. 22020
Pitts, M. C., Poole, L. R., Dörnbrack, A., and Thomason, L. W.: The 2009–2010 Arctic polar stratospheric cloud season: a CALIPSO perspective, Atmos. Chem. Phys., 11, 2161–2177, doi:10.5194/acp-11-2161-2011, 2011. 22018, 22020
Prinn, R. G., Weiss, R. F., Fraser, P. J., Simmonds, P. G., Cunnold, D. M., Alyea, F. N., O'Doherty, S., Salameh, P., Miller, B. R., Huang, J., Wang, R. H. J., Hartley, D. E., Harth, C.,

ACPD
15, 22013–22045, 2015

Steele, L. P., Sturrock, G., Midgley, P. M., and McCulloch, A.: A history of chemically and radiatively important gases in air deduced from ALE/GAGE/AGAGE, J. Geophys. Res., 105, 17751–17792, 2000. 22019

Randel, W., Wu, F., Oltmans, S., Rosenlof, K., and Nedoluha, G.: Interannual changes in stratospheric water vapor and correlations with tropical tropopause temperatures, J. Atmos. Sci., 61, 2133–2148, 2004. 22017, 22025

Sander, S. P., Abbatt, J., Barker, J. R., Burkholder, J. B., Friedl, R. R., Golden, D. M., Huie, R. E., Kolb, C. E., Kurylo, M. J., Moortgat, G. K., Orkin, V. L., and Wine, P. H.: Chemical Kinetics and Photochemical Data for Use in Atmospheric Studies, Evaluation No. 17, JPL Publication 10-6, Jet Propulsion Laboratory, Pasadena, USA, 2011. 22018

Scherer, M., Vömel, H., Fueglistaler, S., Oltmans, S. J., and Staehelin, J.: Trends and variability of midlatitude stratospheric water vapour deduced from the re-evaluated Boulder balloon series and HALOE, Atmos. Chem. Phys., 8, 1391–1402, doi:10.5194/acp-8-1391-2008, 2008. 22017

Schmidt, G. A., Ruedy, R. A., Miller, R. L., and Lacis, A. A.: Attribution of the present-day total greenhouse effect, J. Geophys. Res., 115, D20106, doi:10.1029/2010JD014287, 2010. 22014

Schoeberl, M. R., Dessler, A. E., and Wang, T.: Simulation of stratospheric water vapor and trends using three reanalyses, Atmos. Chem. Phys., 12, 6475–6487, doi:10.5194/acp-12-6475-2012, 2012. 22021

Simmons, A. J., Untch, A., Jakob, C., Kållberg, P., and Undén, P.: Stratospheric water vapour and tropical tropopause temperatures in ECMWF analyses and multi-year simulations, Q. J. Roy. Meteorol. Soc., 125, 353–386, 1999. 22021

Simmons, A. J., Uppala, S. M., Dee, D., and Kobayashi, S.: ERA-Interim: new ECMWF reanalysis products from 1989 omwards, ECMWF Newslett., 110, 25–35, 2007. 22019

Solomon, S., Garcia, R. R., Rowland, F. S., and Wuebbles, D. J.: On the depletion of Antarctic ozone, Nature, 321, 755–758, 1986. 22015

Solomon, S., Rosenlof, K. H., Portmann, R. W., Daniel, J. S., Davis, S. M., Sanford, T. J., and Plattner, G.-K.: Contributions of stratospheric water vapor to decadal changes in the rate of global warming, Science, 327, 5970, 1219–1223, doi:10.1126/science.1182488, 2010. 22015, 22017, 22025

Suortti, T. M., Kats, A., Kivi, R., Kämpfer, N., Leiterer, U., Miloshevich, L. M., Neuber, R., Paukkunen, A., Ruppert, P., Vömel, H., and Yushkov, V.: Tropospheric comparisons of

ACPD
15, 22013–22045, 2015

Vaisala radiosondes and balloon-borne frost-point and lyman-alpha hygrometers during the LAUTLOS-WAVVAP experiment, J. Atmos. Ocean. Tech., 25, 149–166, 2008. 22020

Thölix, L., Backman, L., Ojanen, S.-M.: The effects of driver data on the performance of the FinROSE chemistry transport model, IJRS, 31, 6401–6408, 2010. 22017

Tian, W. S., Chipperfield, M. P., and Lü, D. R.: Impact of increasing stratospheric water vapor on ozone depletion and temperature change, Adv. Atmos. Sci., 26, 423–437, doi:10.1007/s00376-009-0423-3, 2009. 22015

Vömel, H., Oltmans, S. J., Hofmann, D. J., Deshler, T., and Rosen, J. M.: The evolution of the dehydration in the Antarctic stratospheric vortex, J. Geophys. Res., 100, 13919–13926, 1995. 22020, 22026

Vömel, H., Barnes, J., Forno, R., Fujiwara, M., Hasebe, F., Iwasaki, S., Kivi, R., Komala, N., Kyrö, E., Leblanc, T., Morel, B., Ogino, S.-Y., Read, W., Ryan, S. C., Saraspriya, S., Selkirk, H., Shiotani, M., Valverde-Canossa, J., Whiteman, D.: Validation of Aura/MLS water vapor by balloon borne cryogenic frostpoint hygrometer measurements, J. Geophys. Res., 112, D24S37, doi:10.1029/2007JD008698, 2007a. 22019, 22020

Vömel, H., David, D. E., and Smith, K.: Accuracy of tropospheric and stratospheric water vapor measurements by the cryogenic frost point hygrometer: instrumental details and observations, J. Geophys. Res., 112, D08305, doi:10.1029/2006JD007224, 2007b. 22020

Vömel, H., Yushkov, V., Khaykin, S., Korshunov, L., Kyrö, E., and Kivi, R.: Intercomparisons of Stratospheric Water Vapor Sensors: FLASH-B and NOAA/CMDL Frost-Point Hygrometer, J. Atmos. Ocean. Tech., 24, 941–952, 2007c. 22019

ACPD
15, 22013–22045, 2015

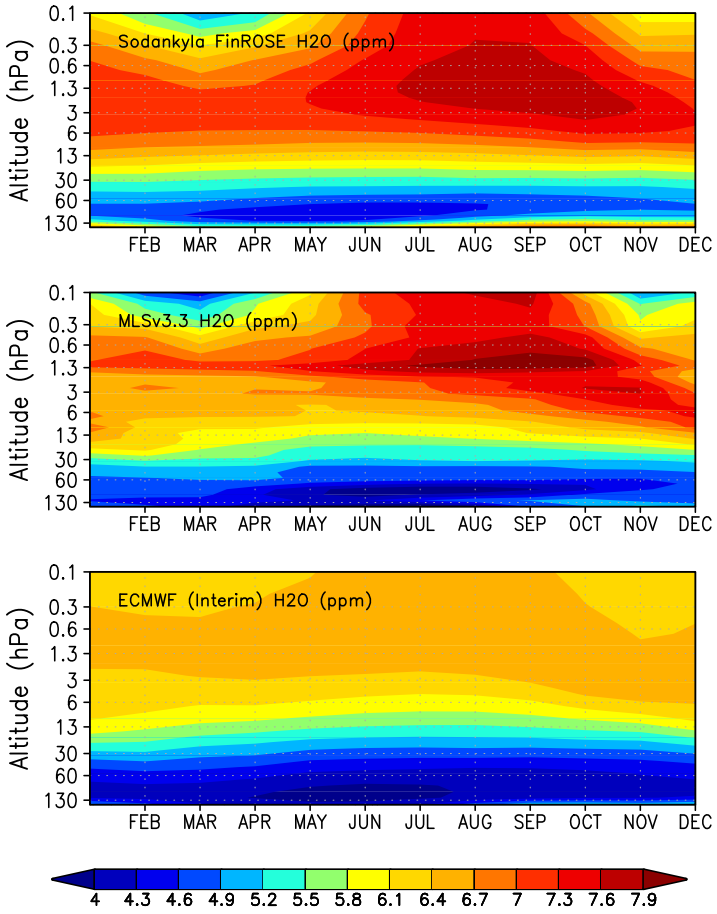

Figure 1. Climatology (2004–2013) of the water vapour distribution from FinROSE, MLS v3.3 data and ECMWF ERA-Interim above Sodankylä.

ACPD
15, 22013–22045, 2015

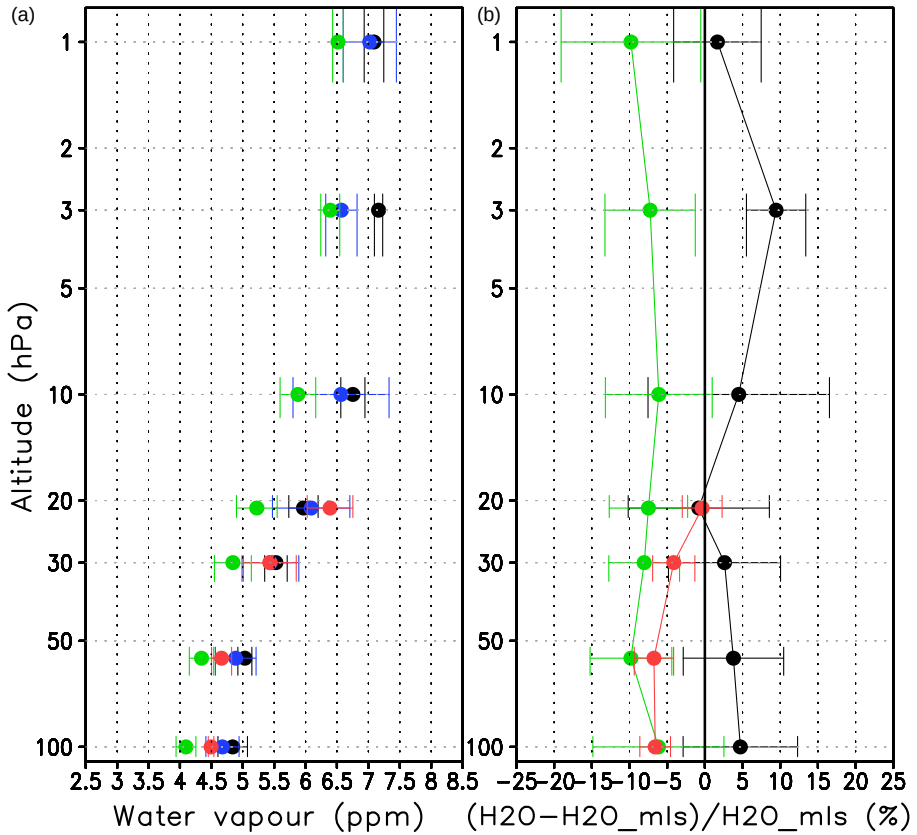

Figure 2. (a) 2010 mean January and February water vapour mixing ratio and standard deviation at different pressure levels above Sodankylä. **(b)** Difference of the modelled or observed winter water vapour mixing ratio and MLS calculated over years 2004 to 2013 at different pressure levels above Sodankylä. FinROSE (black), MLS (blue), ECMWF ERA-Interim (green) and soundings (red).

ACPD
15, 22013–22045, 2015

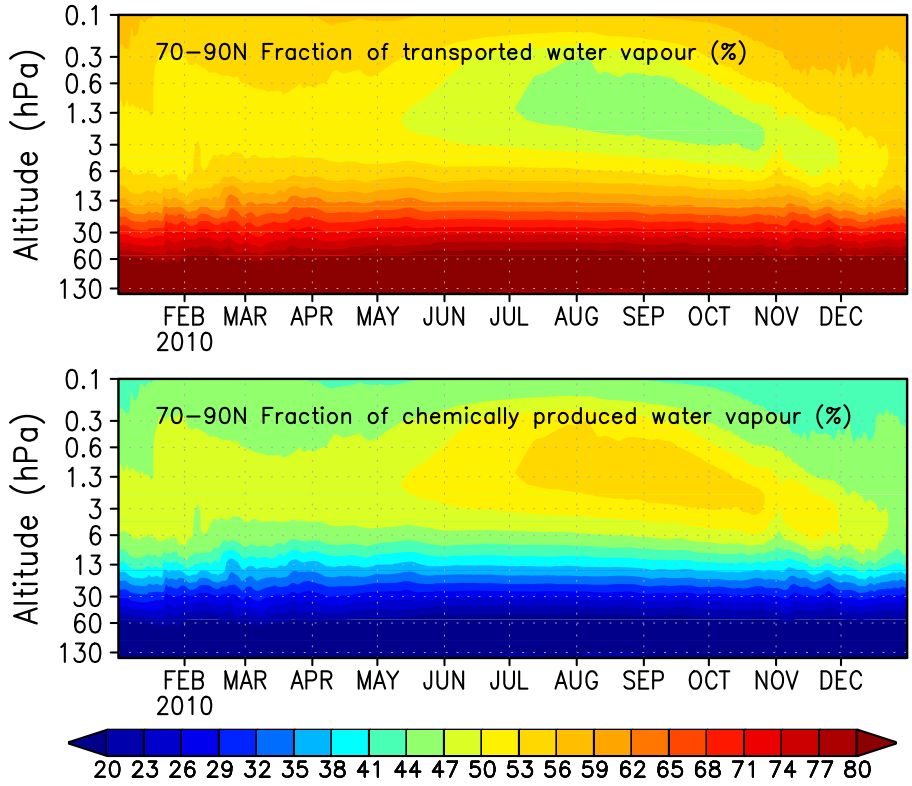

Figure 3. Monthly mean of the fraction of transported water vapour and fraction of chemically produced water vapour (%) for 2010 calculated over 70–90° N.

ACPD
15, 22013–22045, 2015

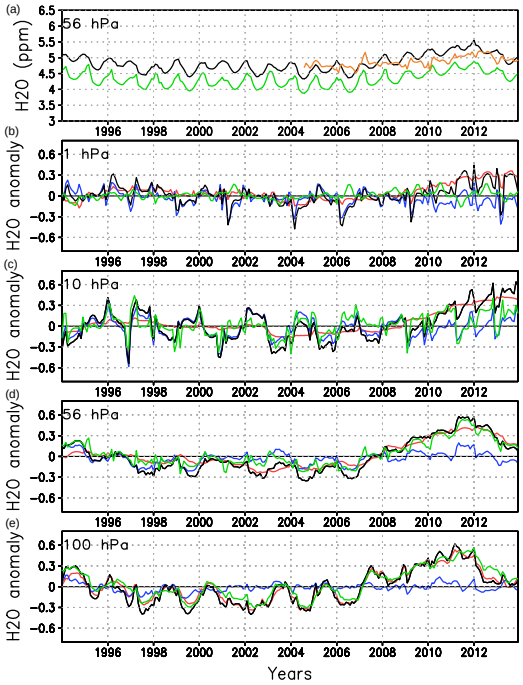

Figure 4. (a) Sodankylä monthly mean water vapour mixing ratio from FinROSE (black), MLS (orange), ECMWF ERA-Interim (green) and soundings (blue dots) at 56 hPa. **(b)** Anomalies of water vapour (black), tracer describing transported water vapour (red), tracer describing water produced by methane oxidation (blue) from FinROSE and water vapour anomaly from ECMWF ERA-Interim (green) as ppm in 1994–2013 at latitudes between 70–90° N at level 1 hPa. **(c–e)** Same as panel **(b)**, but levels 10, 56 and 100 hPa.

ACPD
15, 22013–22045, 2015

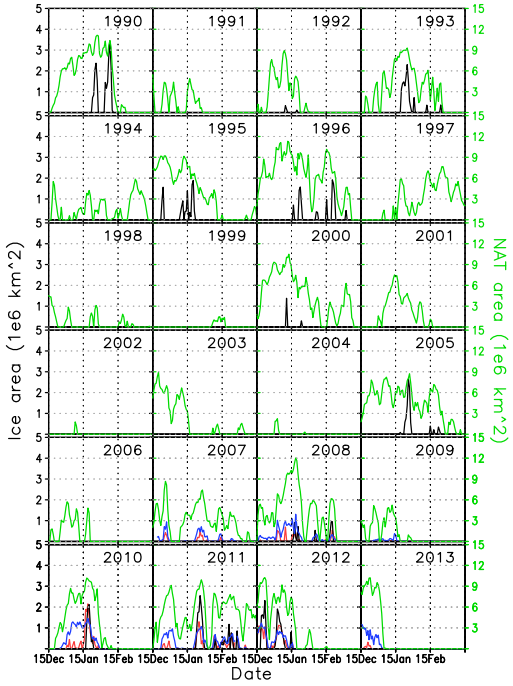

Figure 5. The area of the air mass where ICE and NAT PSCs formed in the FinROSE simulation and was observed by CALIPSO for winters between 1990 and 2013 at 56 hPa. FinROSE ICE area is in black and CALIPSO ICE area is red (left *y* axis). FinROSE NAT area is in green and CALIPSO NAT area in blue (right *y* axis).

ACPD
15, 22013–22045, 2015

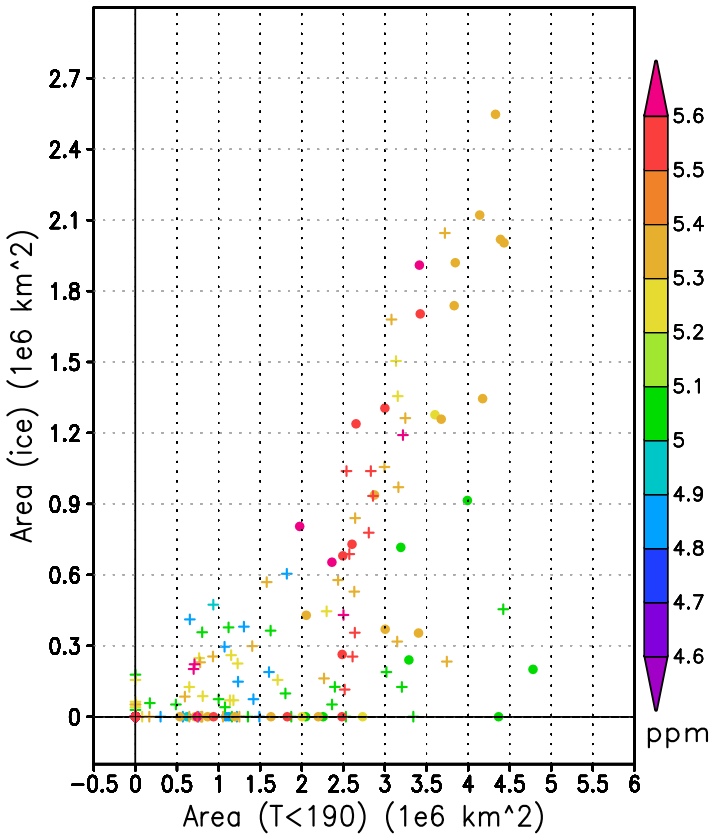

Figure 6. Relation of January ICE PSC area and the area of colder than 190 K in the Northern Hemisphere from FinROSE (points) and CALIPSO (crosses) at 56 hPa level. The colour denotes the vortex average water vapour content.

ACPD
15, 22013–22045, 2015

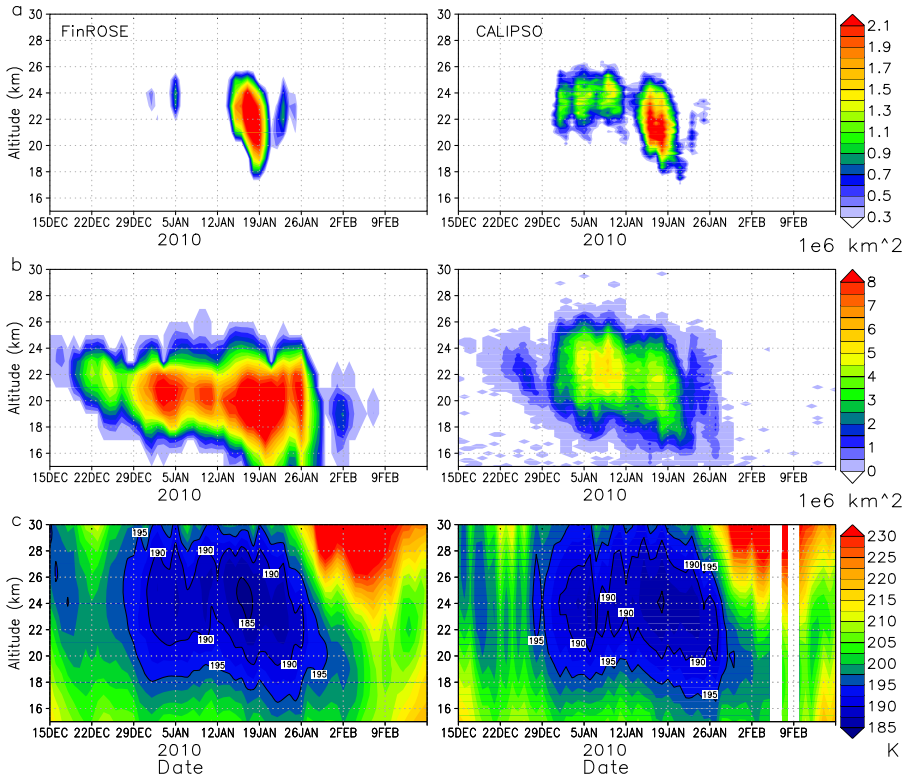

Figure 7. (a) ICE PSC from FinROSE and CALIPSO, **(b)** NAT PSC from FinROSE and CALIPSO and **(c)** temperature from ECMWF ERA-Interim and CALIPSO near Sodankylä in winter 2010.

ACPD
15, 22013–22045, 2015

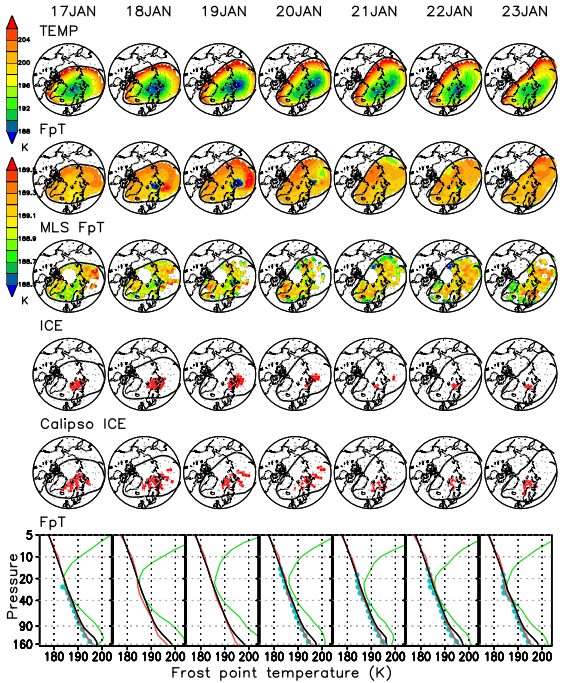

Figure 8. Temperature, frost point temperature (K) and ICE PSC from FinROSE, MLS frost point temperature (K) and CALIPSO ICE PSC occurrence during the extreme cold period of winter 2010 (between 17 and 23 January). The black contour is the border of the vortex defined as modified PV > 36. All the maps are from 56 hPa altitude. Lowest row: ERA-Interim temperature (green), frost point temperature from Sodankylä water vapour soundings (blue dots), from MLS (red) and from FinROSE-ctm (black).

ACPD
15, 22013–22045, 2015